

Active control of light trapping by means of local magnetic coupling

M. Burrese,^{1,*} T. Kampfrath,² D. van Oosten,¹ J. C. Prangsma,¹ B. S. Song,^{3,4} S. Noda,³ and L. Kuipers¹

¹*Center for Nanophotonics, FOM Institute for Atomic and Molecular Physics (AMOLF),
Science Park 113, 1098 XG Amsterdam, The Netherlands*

²*Center for Nanophotonics, FOM Institute for Atomic and Molecular Physics (AMOLF),
Kruislaan 407, 1098 SJ Amsterdam, The Netherlands*

³*Department of Electronic Science and Engineering,
Kyoto University, Kyotodaigaku-Katsura,
Nishikyo-ku, Kyoto 615-8510, Japan.*

⁴*School of Information and Communication,
Sungkyunkwan University, Janan-Gu, Suwon 440-746, Korea.*

(Dated: March 11, 2022)

Abstract

The ability to actively tune the properties of a nanocavity is crucial for future applications in photonics and quantum information. Two important man-made classes of materials have emerged to mold the flow of electromagnetic waves. Firstly, photonic crystals are dielectric nanostructures that can be used to confine and slow down light and control its emission. They act primarily on the electric component of the light field. More recently, a novel class of metallo-dielectric nanostructures has emerged. These so-called metamaterials enable fascinating phenomena, such as negative refraction, super-focusing and cloaking. This second class of materials realizes light control through effective interactions with both electric and magnetic component. In this work, we combine both concepts to gain an active and reversible control of light trapping on subwavelength length scales. By actuating a nanoscale magnetic coil close to a photonic crystal nanocavity, we interact with the rapidly varying magnetic field and accomplish an unprecedented control of the optical properties of the cavity. We achieve a reversible enhancement of the lifetime of photons in the cavity. By successfully combining photonic crystal and metamaterials concepts, our results open the way for new light control strategies based on interactions which include the magnetic component of light.

PACS numbers:

Photonic crystals are materials which provide a high level of control on the light-matter interaction, based on the engineered periodic modulation of the electric permittivity [1]. Nanoresonators in such photonic crystal architectures can store light in volumes comparable to the wavelength cubed for times longer than a million oscillation periods of the light [2]. Such high- Q photonic nano-cavities are promising structures to achieve strong coupling between light and quantum dots [3, 4]. The ability to actively tune the properties of a nanocavity is crucial for future applications in photonics and quantum information [3, 4]. Active tuning is achievable all-optically [5], electrically [6] or through the actuation of nano-objects in the evanescent electromagnetic field of the cavity [7, 8, 9, 10, 11]. The latter strategy, which could lead to breakthroughs in the emerging field of optical nanoelectromechanical systems (NEMS) [12], relies typically on the interaction with the electric field in the cavity. This invariably leads to only red shifts of the resonance frequency and usually to a reduction of the photon lifetime of the cavity [7, 8, 9, 10, 11]. In principle, an interaction with the magnetic field would also allow tuning of the cavity [9]. Unfortunately, natural materials have a negligible magnetic permeability at optical frequencies. We can overcome this limitation by borrowing concepts from metamaterials. These engineered materials work by geometrically inducing a magnetic response [13]. By using this idea, we have achieved active and reversible tuning of a photonic crystal nanocavity by interacting with the magnetic field of the trapped light. We use a cylindrically symmetric, metal-coated probe as a 'nanocoil'. By positioning the probe close to the cavity, the z-component of the magnetic field induces a counteracting magnetic response in the nanocoil through Lenz' law. As a result, we are able to induce a novel blue shift of the resonance frequency. More importantly, we are able to achieve an increase of the quality factor Q . In other words, we are able to increase the photon lifetime in the cavity.

We investigate a photonic crystal nanocavity which is side-coupled to a photonic crystal waveguide (see inset Fig. 1A) [14]. The nanocavity exhibits a resonance at a vacuum wavelength of $\lambda_o = 1534.6$ nm with a quality factor $Q_o = 6500$. In order to excite the cavity, light from a tunable diode laser is coupled to the access waveguide. The electric field distribution inside and around the cavity is detected with a phase-sensitive near-field microscope [15] (Fig. 1A). By raster scanning a tapered aluminum-coated single-mode fibre (Fig. 1B) above the sample at a constant height of 20 nm, we collect a minute fraction of the light and detect it with a heterodyne scheme. The near-field probe, which has an aperture

of 200 nm and an aluminum coating of 100 nm, has a cylindrical symmetry [16]. The high symmetry of the probe allows us to detect the in-plane electric field distribution of the sample [17]. Figure 2A displays the distribution of $\text{Re}(E_y)$ detected with a typical near-field measurement at vacuum wavelength λ_o . The image shows how the electromagnetic wave is guided by the waveguide and is coupled to the cavity, which is indicated by the dashed box in Fig. 2A. Excellent agreement is found between the measured (2B) and the calculated (2C) field distribution above the cavity, obtained by Finite Difference Time Domain (FDTD) method. Small deviations between theory and experiment are visible. The field outside the cavity appears stronger in the measurement than in the calculation, as indicated by the arrows. We assign this effect to the influence of the probe on the optical properties of the cavity, as it will be described later in this chapter.

While performing the near-field measurement, we simultaneously determine the transmission of the system by measuring the amount of light arriving at the output of the access waveguide. In order to investigate the influence of the probe on the transmittance of the system, we determine the normalized transmission $F(x, y, \lambda) = T_n(x, y, \lambda)/T_o(\lambda)$, where x and y represent the in-plane position of the probe, $T_n(x, y, \lambda)$ is the transmission spectrum as a function of probe position above the cavity, and $T_o(\lambda)$ is the unperturbed transmission spectrum obtained in absence of the probe. Figure 3A shows a typical image of this normalized transmission acquired on resonance ($\lambda = \lambda_o$). Different probe positions may lead to either an increase (yellow areas in the image, $F > 1$) or a decrease (blue areas, $F < 1$) of the waveguide transmittance. This observation clearly indicates an interaction between probe and cavity. In addition, we analyze the normalized transmission as a function of wavelength for a fixed position of the probe. The upper image of Fig. 3B shows a typical graph of F for position 1 in Fig. 3A, whereas the lower image shows F for 3 other positions indicated in Fig. 3A. All spectra exhibit identical qualitative behavior. For wavelengths far away from the resonance, the influence of the probe is negligible, i.e. $F = 1$. For wavelengths close to λ_o , the probe-cavity interaction becomes evident since F undergoes a pronounced variation. The change in transmission is caused by a shift of the resonance ($\lambda_o \rightarrow \lambda_n(x, y)$) due to the probe-cavity coupling [7, 9], as a consequence of which light with wavelength λ_o no longer couples to the resonator. As a result, the light does not experience the small loss associated with being trapped in the cavity and the transmission increases. Conversely, light with a wavelength close to the new resonance λ_n is now loaded in the resonator, leading to

a reduction of the transmittance for that wavelength. It is clear that a distinct blue-shift of the cavity resonance occurs when the near-field probe couples to the cavity.

The induced resonance shift is the cause of the above-mentioned disagreement between Fig. 2B and C. When the probe is above the cavity, light with wavelength λ_o is not loaded and the electric field in the resonator is smaller than in the unperturbed system. Conversely, when the probe is at the position indicated by the arrow in Fig. 2B, light with wavelength λ_o can couple to the nanocavity and the electric field at that location, as well as the signal detected by the probe, increases. As a result, the ratio between the electric field amplitude inside and outside the cavity for the measurement (Fig. 2B) differs from the same ratio for the calculation (Fig. 2C).

This unprecedented blue-shift can be intuitively understood in the following way. Due to the small extension in air of the evanescent fields above the cavity [18], the end of our near-field probe can be modeled as a metallic ring (Fig. 1C) that acts like a nano-coil in the electromagnetic field above the cavity. Faraday's law tells us that the magnetic field induces a circular current density \mathbf{J}_p in the ring (Fig. 1C). This current, in turn, generates a magnetic field that, according to Lenz' law, suppresses the driving field inside the ring [19]. The probe, thus, generates a volume where the total magnetic field is reduced. As a result, the effective volume occupied by the light stored in the cavity, the so-called cavity mode volume, is reduced, leading to a resonance shift towards shorter wavelengths.

As a consequence, we expect that the probe-cavity coupling, and thus the variation of the transmittance, is most pronounced when the probe overlaps with the maximum in the amplitude of the out-of-plane component of the magnetic field. We experimentally verify our expectations by comparing the normalized transmission map, shown in Fig. 3A, with the amplitude distribution of B_z , obtained by FDTD calculation and shown in Fig. 4B. The symmetry and the maxima of the transmission map do coincide with the amplitude of B_z and not with the magnitude of the electric field \mathbf{E} (Fig. 4A). This indication proves that the probe-cavity interaction is dominated by the magnetic coupling.

For a more formal description of the probe-cavity interaction one has to consider that the relative resonance shift is proportional to the relative energy shift of the system [7, 9]. Here, we have to take into account the induced magnetic dipole moment \mathbf{m} of the probe interacting with the magnetic field in addition to the coupling between the induced electric dipole moment \mathbf{p} of the probe and the electric field. Therefore, the resonance shift can be

written as:

$$\frac{\Delta\omega_o}{\omega_o} = -\frac{\mathbf{E}_o^* \cdot \mathbf{p} + \mathbf{B}_o^* \cdot \mathbf{m}}{2U_E}, \quad (1)$$

where ω_o is the resonant angular frequency of the system, $2U_E$ is the total energy stored in the cavity. The dipole moments, in turn, are proportional to the unperturbed \mathbf{E}_o and \mathbf{B}_o and can be expressed as $p_i = \alpha_{ii}^{ee} E_i$ and $m_i = \alpha_{ii}^{mm} B_i$, where the label i indicates the spatial coordinates x , y and z . The proportionality constants α_{ii}^{ee} and α_{ii}^{mm} are the electric and magnetic polarizabilities of the probe, respectively. From eq. 1 it is clear that when the perturbative object only exhibits an electric response, the transmittance variation were largest when the probe overlaps with the amplitude maxima of the electric field [7, 8, 9, 10, 11]. In order to calculate the electric polarizabilities, we can approximate the ring as a metallic oblate spheroid, following the methodology often employed in split-ring resonators [20]. The electric polarizabilities turn out to be positive. The magnetic polarizability can be calculated by applying Faraday's law to a single metallic loop. This leads to a negative polarizability $\alpha_{zz}^{mm} = -A^2/(L + iR/\omega)$, where L is the self-inductance of the ring, R is the complex Ohmic resistance and r_2 is the outer radius. Besides exhibiting a positive electric polarizability, our near-field probe also has a negative magnetic polarizability. Thus, the electric coupling $\mathbf{E}_o \cdot \mathbf{p} > 0$ induces a red-shift [7, 8, 9, 10, 11], whereas the magnetic coupling $\mathbf{B}_o \cdot \mathbf{m} < 0$ leads to a blue-shift. Thus, when the magnetic coupling dominates the resonance is primarily blue-shifted.

In order to compare the theoretical prediction of eq. 1 to our experimental data, we extract the relative shift $\Delta\lambda/\lambda_o$ from our measurements. For this purpose, we fit a transmission function based on coupled-mode theory [21] to the normalized transmission. Figure 3B shows a typical fit as a red line. From the fit we obtained the relative resonance shift $\Delta\lambda/\lambda_o$ and the relative change in the quality factor $\Delta Q/Q_o$ for all probe positions. In Fig. 5A we show the measured $\Delta\lambda/\lambda_o$ as a function of the probe position. By comparing with Fig. 3A, it is evident that the largest relative blue-shifts, of the order of 10^{-4} , occur for positions of the probe where the amplitude of B_z is maximum. We calculate the resonance shift by using eq. 1 and the field distributions inside the cavity, which were obtained by FDTD calculations. In order to take into account the finite size of the probe, we use the average electric and magnetic fields over the area of the ring by making a convolution of the probe apex shape with the calculated field distributions. The theoretically obtained $\Delta\lambda/\lambda_o$ is shown in Fig. 5B. We find an excellent qualitative agreement with the experimental data

(Fig. 5A).

In addition to tuning the resonance frequency, we also control the lifetime of the photons in the cavity. In Fig. 6A, we show an image of the retrieved $\Delta Q/Q_o$ as a function of the probe position. Remarkably, the relative change in Q can, depending on the probe position, be both positive and negative! The largest increase of Q of 50% occurs right above the amplitude maxima of B_z , co-located with the largest blue-shift. The magnetic coupling between the probe and the cavity, thus, not only induces a novel blue-shift of the resonance but also causes the photon lifetime in the cavity to be increased.

Any 2D cavity is affected by losses due to intrinsic out-of-plane radiation [14]. In a previous study, Robinson *et al* [22] reported an increase of only 1% of Q of a nanocavity which resulted from the destructive interference between the out-of-plane radiation and its back-reflection from a metallic object much larger than the nanocavity itself. However, to significantly improve the Q , one has to destructively interfere with a larger amount of the out-of-plane radiation. We achieve 50% increase of the photon lifetime by exploiting the emission caused by the magnetic dipole moment of the probe. In fact, this induced dipole moment emits primarily along the surface of the sample in counter phase with respect to the driving field inside the cavity. On the other hand, as shown by Fourier analyses performed on the cavity mode [14], the cavity also radiates along the surface. We detected this radiation during a near-field measurement, as indicated by the green arrows in Fig. 2A where. Therefore, the in-plane radiation of the cavity and the emission from the probe destructively interfere (the process is schematically described in Fig. 6B). Moreover, analyses on the in-plane decay rate show that we increase the quality of the cavity by also decreasing the coupling with the access waveguide. Remarkably, we obtain a pronounced increase of Q by exploiting at the nano-scale the scattered light from an object smaller than the nanocavity. Furthermore, we achieve an increase of the lifetime by means of magnetic coupling rather than electric.

Here, we have experimentally demonstrated that we can actively and reversibly control the trapping of light in a photonic crystal nanocavity by means of magnetic coupling with an actuated subwavelength object. The presented method opens up a new way for light control, combining photonic crystals and metamaterials concepts. Moreover, a new exciting application for photonic crystal nanocavities arises. We anticipate the possibility of measuring the magnetic dipole moment of magnetically resonant nano-object, such as single split-ring resonator [23] or single twisted split-ring resonator dimers [24], by actuating it above a max-

imum of the magnetic field of the nanoresonator. Along these lines, we also envision the striking possibility of using a state-of-the-art ultra-high- Q [2] nanocavity, characterized by a sharp resonance, for measuring the minute magnetic susceptibility of molecules, such as carbon nanotubes [25] or ring-shape (aromatic) molecules [26].

This manuscript is extracted by the Ph.D. dissertation of M. Burrese. We wish to thank H. Schoenmaker for technical support and M. Bonn and G. H. Koenderink for helpful discussion and support. This work is part of the research program of the "Stichting voor Fundamenteel Onderzoek der Materie (FOM)", which is financially supported by the "Nederlandse organisatie voor Wetenschappelijk Onderzoek (NWO)". Support by the NWO (VICI grant) is gratefully acknowledged. This work is also supported by NanoNed, a nanotechnology program of the Dutch Ministry of Economic affairs.

* burrese@amolf.nl, burrese@lens.unifi.it

- [1] Yablonovitch, E. Inhibited spontaneous emission in Solid-State physics and electronics. *Phys. Rev. Lett.* **58**, 2059 (1987).
- [2] Takahashi, Y. *et al.* High- Q nanocavity with a 2-ns photon lifetime. *Opt. Express* **15**, 17206–17213 (2007).
- [3] Yoshie, T. *et al.* Vacuum rabi splitting with a single quantum dot in a photonic crystal nanocavity. *Nature* **432**, 200–203 (2004).
- [4] Hennessy, K. *et al.* Quantum nature of a strongly coupled single quantum dot-cavity system. *Nature* **445**, 896–899 (2007).
- [5] Almeida, V. R., Barrios, C. A., Panepucci, R. R. & Lipson, M. All-optical control of light on a silicon chip. *Nature* **431**, 1081–1084 (2004).
- [6] Xu, Q., Schmidt, B., Pradhan, S. & Lipson, M. Micrometre-scale silicon electro-optic modulator. *Nature* **435**, 325–327 (2005).
- [7] Koenderink, A. F., Kafesaki, M., Buchler, B. C. & Sandoghdar, V. Controlling the resonance of a photonic crystal microcavity by a Near-Field probe. *Phys. Rev. Lett.* **95**, 153904 (2005).
- [8] Hopman, W. C. L. *et al.* Nano-mechanical tuning and imaging of a photonic crystal microcavity resonance. *Opt. Express* **14**, 8745–8752 (2006).
- [9] Lalouat, L. *et al.* Near-field interactions between a subwavelength tip and a small-volume

- photonic-crystal nanocavity. *Phys. Rev. B* **76**, 41102 (2007).
- [10] Mujumdar, S. *et al.* Near-field imaging and frequency tuning of a high-Q photonic crystal membrane microcavity. *Opt. Express* **15**, 17214–17220 (2007).
- [11] Intonti, F. *et al.* Spectral tuning and near-field imaging of photonic crystal microcavities. *Phys. Rev. B* **78**, 041401–4 (2008).
- [12] Li, M. *et al.* Harnessing optical forces in integrated photonic circuits. *Nature* **456**, 480–484 (2008).
- [13] Soukoulis, C. M., Linden, S. & Wegener, M. Negative refractive index at optical wavelengths. *Science* **315**, 47–49 (2007).
- [14] Akahane, Y., Asano, T., Song, B. S. & Noda, S. High-Q photonic nanocavity in a two-dimensional photonic crystal. *Nature* **425**, 944–947 (2003).
- [15] Balistreri, M. L. M., Gersen, H., Korterik, J. P., Kuipers, L. & van Hulst, N. F. Tracking femtosecond laser pulses in space and time. *Science* **294**, 1080–1082 (2001).
- [16] Veerman, J. A., Otter, A. M., Kuipers, L. & van Hulst, N. F. High definition aperture probes for near-field optical microscopy fabricated by focused ion beam milling. *App. Phys. Lett.* **72**, 3115 (1998).
- [17] Burrelli, M. *et al.* Observation of polarization singularities at the nanoscale. *Phys. Rev. Lett.* **102**, 033902 (2009).
- [18] Engelen, R. J. P., Mori, D., Baba, T. & Kuipers, L. Subwavelength structure of the evanescent field of an optical bloch wave. *Phys. Rev. Lett.* **102**, 023902 (2009).
- [19] Landau, L. D. & Lifshitz, E. M. *Electrodynamics of continuous media* (Wiley, 1984).
- [20] Marques, R., Medina, F. & Ruffino-El-Idrissi, R. Role of bianisotropy in negative permeability and left-handed metamaterials. *Phys. Rev. B.* **65**, 144440–144440 (2002).
- [21] Manolatou, C. *et al.* Coupling of modes analysis of resonant channel add-drop filters. *IEEE J. Quantum Electron.* **35**, 1322–1331 (1999).
- [22] Robinson, J. T. & Lipson, M. Far-Field control of radiation from an individual optical nanocavity: Analogue to an optical dipole. *Phys. Rev. Lett.* **100**, 043902–4 (2008).
- [23] Husnik, M. *et al.* Absolute extinction cross-section of individual magnetic split-ring resonators. *Nature Photon.* **2**, 614–617 (2008).
- [24] Liu, N., Liu, H., Zhu, S. & Giessen, H. Stereometamaterials. *Nature Photon.* **3**, 157–162 (2009).

- [25] Minot, E. D., Yaish, Y., Sazonova, V. & McEuen, P. L. Determination of electron orbital magnetic moments in carbon nanotubes. *Nature* **428**, 536–539 (2004).
- [26] Haddon, R. C. Magnetism of the carbon allotropes. *Nature* **378**, 249–255 (1995).

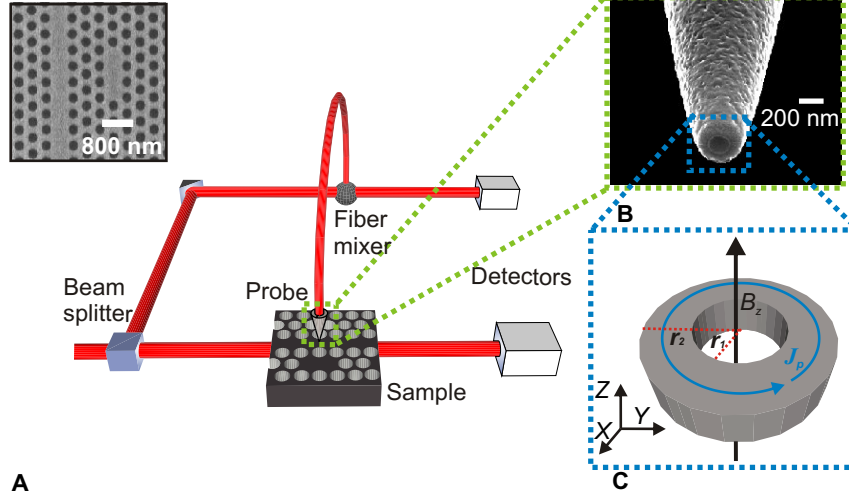


FIG. 1: **A**, The near-field probe is scanned above the sample and collects the evanescent field of the light in the structure. The collected light is mixed with a reference beam and subsequently detected with a heterodyne scheme. The light power transmitted by the structure is also detected. A scanning electron micrograph of the sample investigated is shown in the inset. The photonic crystal nanocavity is visible below the photonic crystal waveguide. **B**, A scanning electron micrograph of the cylindrical symmetric aluminium-coated near-field probe. **C**, Schematic representation of the ring that models the end of the near-field probe. The magnetic field B_z , that is orthogonal to the ring, induces a current density J_p in the ring. r_1 and r_2 are the outer and the inner radius, respectively.

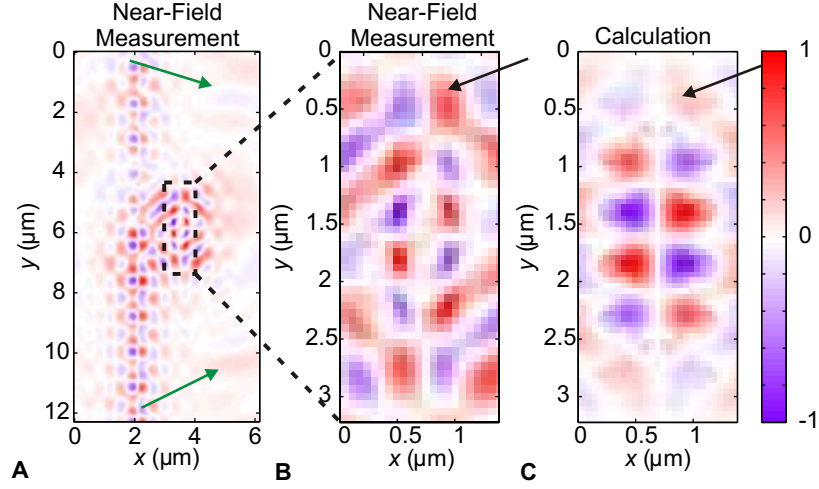


FIG. 2: **A**, Distribution of $\text{Re}(E_y)$ detected in the near field of the sample at resonance. The electromagnetic field depicted here is propagating through the accessing waveguide and coupled to the cavity. The color scale is varying between the maximum (red-positive) and the minimum (violet-negative) of the interference signal. **B**, Image of the distribution of the detected $\text{Re}(E_y)$ in the near field above the area indicated in the dashed box of Fig. 2A. The green arrows indicate the detected in-plane radiation lost by the cavity. **C**, Image of the calculated distribution of the longitudinal component obtained by FDTD calculations at resonance.

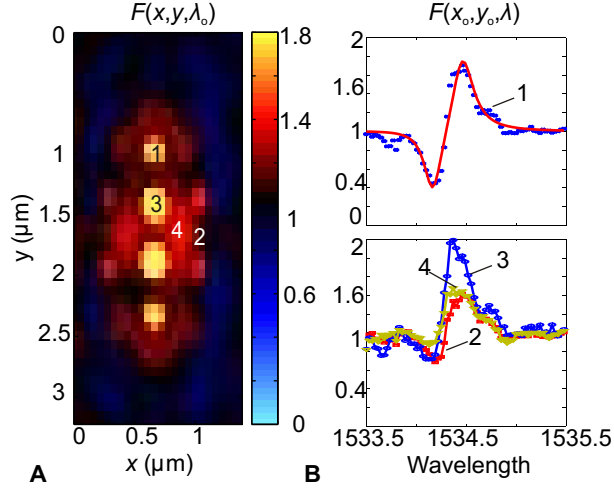


FIG. 3: **A**, Image of the normalized transmission at resonance. In black the areas where the transmittance equals the unperturbed transmittance. For different positions of the probe the transmittance either increases or decreases. **B**, In the upper image the normalized transmission F for position 1 in Fig. 3A is shown. For wavelengths far away from the resonance the ratio is 1, indicating no influence of the probe. However, for wavelengths close to the resonance this ratio varies drastically. The fit is shown as a red line. The lower image shows F obtained for different positions indicated in Fig. 3A.

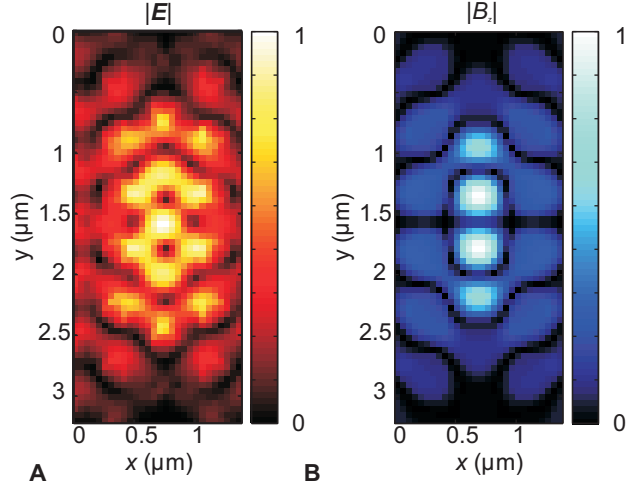


FIG. 4: **A** and **B**, Distribution of the magnitude of the electric field \mathbf{E} and of the amplitude of the vertical component of the magnetic field B_z normalized to their maximum, respectively. The area shown is the same as Fig. 3A. The two pictures show a different symmetry in the pattern of the field distributions.

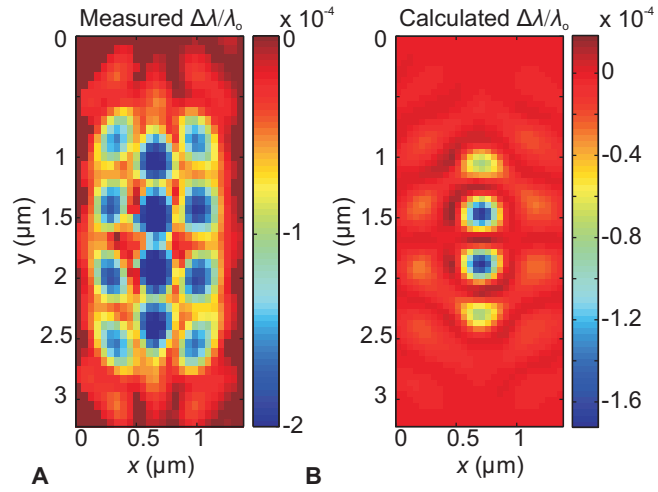


FIG. 5: **A** and **B**, Images of the measured and calculated shift of the resonance $\Delta\lambda_0/\lambda_0$ at every probe position. Figure 5A shows an evident blue-shift of the resonance when the probe is above maxima of the $|B_z|$. We find an excellent quantitative agreement with the calculated resonance shift in Fig. 5B.

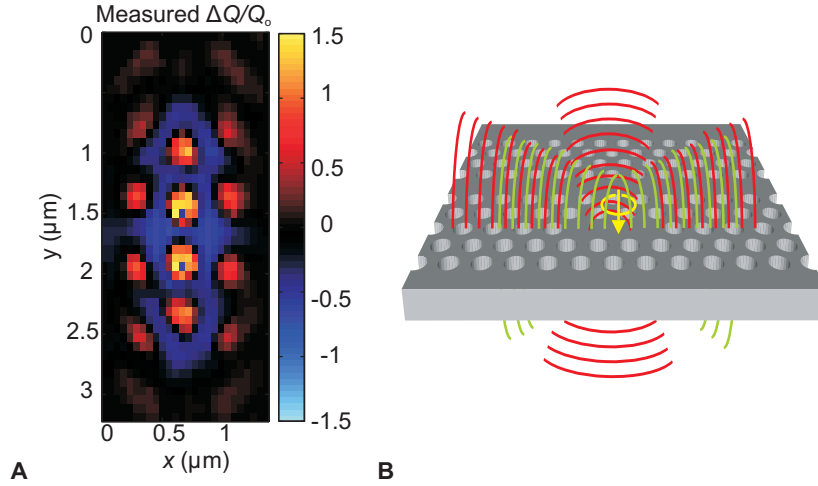


FIG. 6: **A**, Image of the measured shift of the quality factor $\Delta Q/Q_0$ at every probe position. An increase and the decrease of the quality factor of the cavity is evident. **B**, Representation of the proposed mechanism that causes the increase of the quality factor. As the probe is above a maximum of the magnetic field, the induced current generates radiation that destructively interferes with the radiative loss of the cavity, yielding an increase of the photon lifetime.